Photorefractive Amplification at High Frequencies

Russell M. Kurtz* (Life Member, SPIE), Weixing Lu, Judy Piranian
RAN Science & Technology, LLC
609 Deep Valley Dr. Ste. 200, Rolling Hills Estates, CA 90274

Albert O. Okorogu (Member, SPIE)
The Aerospace Corporation
P.O. Box 92957, Los Angeles, CA 90009

ABSTRACT

Photorefractive optical amplification, while useful, is a slow process. Under some circumstances, however, it amplifies optical signals effectively even when one is modulated at a relatively high frequency. We determine the reasons for this capability (what we have called the "Fast Photorefractive Effect") and analyze its enhanced bandwidth, improvements over standard photorefractivity, and limitations.

1. Introduction

Photorefractivity is a well-known optical amplification system, high gain[1, 2] and low noise[3, 4]. It is generally considered to be a slow process, whether limited by the power of the writing beams or the characteristics of the photorefractive material[5]. Typical values of the grating writing or erase speed in, for example, $BaTiO_3$, are 0.1-10 s (over a beam irradiance range 0.1-10 W/cm^2)[6]. For Cu:$(K_xNa_{1-x})_{2a}(Sr_yBa_{1-y})_{1-a}Nb_2O_6$ (Cu:KNSBN), the writing speed typically runs from 0.2-1 s over this same irradiance range[7, 8]. If the amplification properties of the photorefractive material requires rewriting the grating, then, these materials limit the amplification bandwidth to <10 Hz. Our initial experiments with Cu:KNSBN, however, demonstrated an amplification bandwidth exceeding 1 MHz[9]. We detected very small photorefractive amplification of signals at even larger frequency offsets, even as great as 73 THz (reference at 532 nm, signal at 612 nm, amplified signal at 532 nm), although signals at 10 THz offset and larger were only slightly amplified.

Further experimentation demonstrated that our photorefractive amplifier had power gain between 30 and 35 over the frequency range dc-4.0 MHz (limited by the modulator). The experiments showed that the high frequency gain was only seen in phase-modulated (vibration-like) signals, rather than frequency-modulated (communication-like) signals. A redesign of the system, producing a static grating in the photorefractive crystal, demonstrated amplification of frequency-modulated signals with bandwidth approaching that of the phase-modulated signals. Pouet *et al*. demonstrated photorefractive amplification with at least 70 MHz bandwidth in $Bi_{12}SiO_{20}$ (BSO) and $Bi_{12}GeO_{20}$ (BGO), with a static photorefractive grating[10]. We have also determined the mechanism of this Fast Photorefractive Effect, and present a theory predicting its limits.

2. Background and Theory

2.1. Photorefractivity

The basic theory of photorefractive amplification is contained in the Standard Model of Photorefractivity (STPM)[11, 12]. According to the STPM, a photorefractive material essentially acts as a doped semiconductor (Fig. 1). The host material bandgap must be large enough that it is transparent at the wavelength to be used for photorefractivity. The dopant bandgap, however, must be less than this wavelength. Ideally, the illumination wavelength is sufficient to excite a dopant into the host material conduction band (assuming the carriers are electrons). Then it is possible to trap the excited ion in a trapping level, where the dark lifetime is long. The dopant is ionized where the illumination is strongest; if the illumination is in the form of a sinusoidal grating, the excited ions are formed in the bright regions. They do not collect in these areas, however, since the illumination can deexcite them as easily as it excited them. Some of the excited ions, however, diffuse to areas where the illumination is dark. These can maintain their excitation for long periods.

* Corresponding author, russell.kurtz@ranscitech.com, phone (310) 265-4448, fax (310) 265-4449

Practical Holography XXV: Materials and Applications, edited by Hans I. Bjelkhagen,
Proc. of SPIE Vol. 7957, 79570K · © 2011 SPIE · CCC code: 0277-786X/11/$18 · doi: 10.1117/12.875761

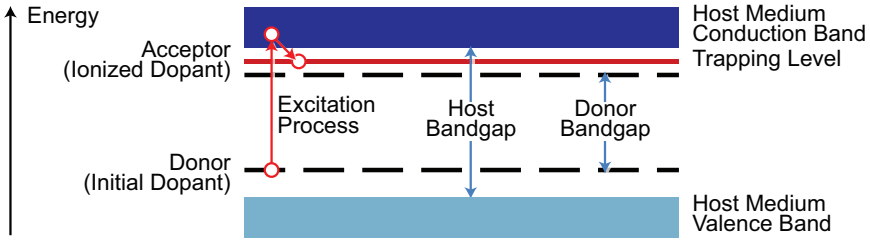

Fig. 1. Energy Diagram for Photorefractive Material.

With illumination due to a sinusoidal grating, then, the electrons ionized from the dopant into trapping levels collect in the darker areas; at low levels of excitation, the increase in electron density very roughly approximates the negative of the grating – so the electric field induced by these moved charges (the space-charge field) roughly approximates the illumination irradiance. If the illumination grating is static, the space-charge field is also static.

Another requirement on the host is to have a large first-order electro-optic effect. The sinusoidal space-charge field then induces a sinusoidal modulation of the refractive index of the host material, creating a grating in the refractive index, which then functions as a phase grating (since optical path length—and, thus, the phase of a beam passing through that area—is just the refractive index multiplied by the physical path length). The photorefractive medium is likely to be optically thick, so the space-charge induced phase grating is simply a thick Bragg grating. It can then be analyzed using standard Bragg grating techniques.

2.2. Phase Modulation *vs.* Frequency Modulation

A key discovery of the Fast Photorefractive Effect is that, in the case of two-beam mixing, it applies to phase-modulated signals only, not frequency-modulated. Since the initial recognition of this effect was in studying vibrometry, it was necessary to understand the reason behind this difference. To do so, we first study the difference between these two types of modulation, what can cause them, and what the difference is in their effects.

For simplicity we describe a simple experiment that can use either phase or frequency modulation (Fig. 2). A coherent illumination beam (from a laser) is passed through a beamsplitter that, in this layout, reflects the vast majority of the beam into the reference and transmits only a small part (the signal). The signal is then modulated by either a phase modulator or a frequency modulator. Two turning mirrors direct the signal to meet the reference; the two beams overlap inside the photorefractive material. The amplified signal is then measured at the readout screen.

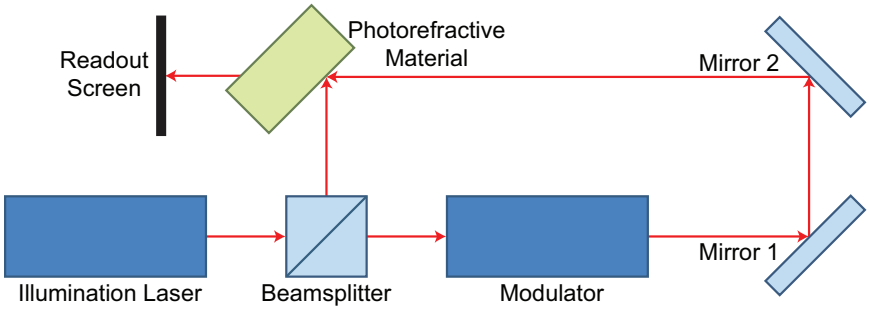

Fig. 2. Modulation Measurement Experiment Concept.

The initial beam, modeled as a single-frequency laser, satisfies the equation

$$E_0(z,t) = A\exp\left[-i(\omega t - kz)\right], \tag{1}$$

where the amplitude is A, the frequency is $\nu \equiv \omega/2\pi = c/\lambda$, the initial beam propagates in the +z-direction, and the propagation is in air so the propagation constant is $k = 2\pi / \lambda$. The beam reflected from the beamsplitter (the reference) then propagates in the +x direction. Since eq. (1) implicitly defines $z = 0$ as the origin of the laser beam, the equation of the reference beam is

$$E_R(x,t) = RA\exp\left[-i\left(\omega t - kz_0 - kx\right)\right], \tag{2}$$

where R is the reflectance of the beamsplitter and $(x, z) = (0, z_0)$ is the location of the beamsplitter. The portion of the beam transmitted by the beamsplitter is then

$$E_1(z,t) = (1-R)A\exp\left[-i\left(\omega t - kz\right)\right]. \tag{3}$$

The beam after the modulator depends on the type of modulation. For frequency modulation at offset $\Delta\omega$, it is

$$E_{FM}(z,t) = (1-R)A\exp\left\{-i\left[\left(\omega + \Delta\omega\right)t - kz\right]\right\}, \tag{4}$$

while a phase-modulated beam with offset $\varphi(t)$ is

$$E_{PM}(z,t) = (1-R)A\exp\left\{-i\left[\omega t - kz - \varphi(t)\right]\right\}. \tag{5}$$

Assuming perfectly reflecting mirrors, the signal beam entering the photorefractive crystal will then be described by the equation

$$E_{S,FM}(z,t) = (1-R)A\exp\left\{-i\left[\left(\omega + \Delta\omega\right)t + kz - kx_0\right]\right\} \tag{6}$$

(the sign change on kz is a result of the change in direction) or

$$E_{S,PM}(z,t) = (1-R)A\exp\left\{-i\left[\omega t + kz - kx_0 - \varphi(t)\right]\right\}. \tag{7}$$

Eqs. (6-7) assume that the offset between the outgoing and returning signal beams is x_0. The capability of the grating to form, and therefore the photorefractive amplification, will depend on the difference in frequency between E_R and E_S[13]. The reference beam operates at a single frequency, ω. The frequency-modulated signal beam also operates at only a single frequency, $\omega + \Delta\omega$. Clearly, the frequency difference between these two beams is $\Delta\omega$. The grating formed within the photorefractive medium will be a "running grating" at frequency $\Delta\omega$.

The situation is different, however, with the phase-modulated signal of eq. (7). To determine the frequency shift of this beam it is necessary to decompose the phase modulation into its frequency components. We know that we can define $\varphi(t)$ in terms of its Fourier components. For simplicity, and because it describes a common vibrational case, we assume

$$\varphi(t) = ka\sin\left(\omega_V t\right), \tag{8}$$

in other words, that the phase modulation is sinusoidal. The parameter a can be the amplitude of the specific Fourier component. Using eq. (8), then, the relevant part of eq. (7) is

$$E_{PM,rel} = \exp\left[ika\sin\left(\omega_V t\right)\right]. \tag{9}$$

Eq. (8) can be decomposed into frequency components using Jacobi-Anger expansion (which is the Fourier sum that results in the exponential)[14],

$$\exp\left(i\zeta\sin\theta\right)=\sum_{m=-\infty}^{\infty}J_m\left(\zeta\right)\exp\left(im\theta\right), \tag{10}$$

where $J_m(\zeta)$ is the m^{th}-order Bessel function of the first kind. Clearly, translating from eq. (9) to eq. (10), $\zeta = ka$ and $\theta = \omega_V t$. In other words, we can decompose eq. (9) into

$$\exp\left[ika\sin\left(\omega_V t\right)\right]=\sum_{m=-\infty}^{\infty}J_m\left(ka\right)\exp\left(im\omega_V t\right), \tag{11}$$

the Fourier decomposition with amplitudes $J_m(ka)$ and frequencies $m\omega_V t$. Thus, while frequency modulation results in a single running grating at frequency $\Delta\omega$, phase modulation results in an infinite sum of gratings at frequencies $m\omega_V$, where m runs from $-\infty$ to ∞.

The Bessel function of the first kind has two interesting properties that affect this analysis. First, only J_0 has any amplitude at 0; $J_m(0) = 0$ for $m \neq 0$. In other words, very small vibrations produce only the zero-frequency component of eq. (11). Second, in general, the amplitude of $J_m(z)$ decays as e^{-m} (Fig. 3); even in relatively large vibration, around half the total power of this frequency decomposition occurs in the zero-frequency component. Thus, if the signal is phase-modulated, there will always be a large component that forms a static grating when forming an interference pattern with the reference. This static grating, then, becomes the main photorefractive grating; the portions of the signal that are at other frequencies can still be amplified, as described in Section 2.3.

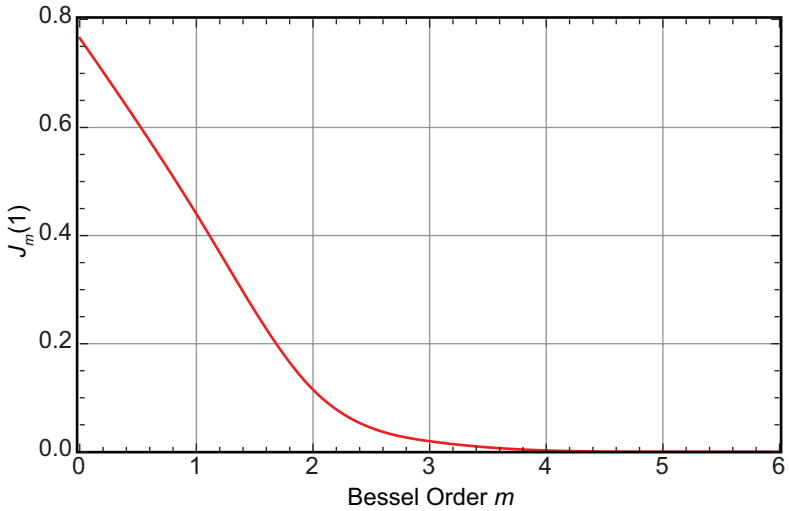

Fig. 3. Bessel Amplitude as a Function of Order.

2.3. Kogelnik's Theory of Bragg Gratings

In 1969, Kogelnik published the theory of beams diffracted from a thick sinusoidal grating[15], which he called a "hologram grating." This theory can be applied to photorefractive materials, as long as the following three assumptions can be made:

1. The modulation of the refractive index is small. Specifically, if we write $n = n_0 + n_1\cos\left(2\pi\zeta/\Lambda\right)$, where n_0 is the refractive index in the absence of illumination, ζ is the length along the grating gradient, and Λ is the grating period, the modulation must satisfy $n_1 \ll n_0$.

2. The grating is almost a pure phase grating, with low absorption in the material. If α is the absorptivity, the material must satisfy $\alpha \ll 2\pi n_0 / \lambda$.
3. The grating is sinusoidal. This assumption is valid as long as the ionized population is small compared to the overall dopant population. If N_0 is the total dopant population, and N_1 is the population of dopant in the trapping levels, this requirement means $N_1 \ll N_0$.

If we further assume that the reference and signal beams are meeting near the Bragg angle—guaranteed for the photorefractive effect using beams at the same wavelength—there is perfect coupling between the beams. In the ideal case, the two beams themselves are each 90° out of phase with the grating; one is 90° advanced, the other 90° retarded. Then power will be transferred with the highest efficiency from the advanced beam to the retarded beam. This is clear from eq. (4-7); if the beam phase is 90° advanced, k becomes ik, and the exponential includes a term e^{-kz}. Likewise, the retarded beam includes a term e^{+kz}. This is the source of the power transfer from the reference to the signal beam (if the photorefractive amplifier is set up correctly.

Given that the photorefractive amplifier meets the three requirements listed above, Kogelnik's theory can be combined with the STPM to determine the single-pass, two-beam amplification through a photorefractive amplifier. Fig. 4 shows the geometry used in the following calculations.

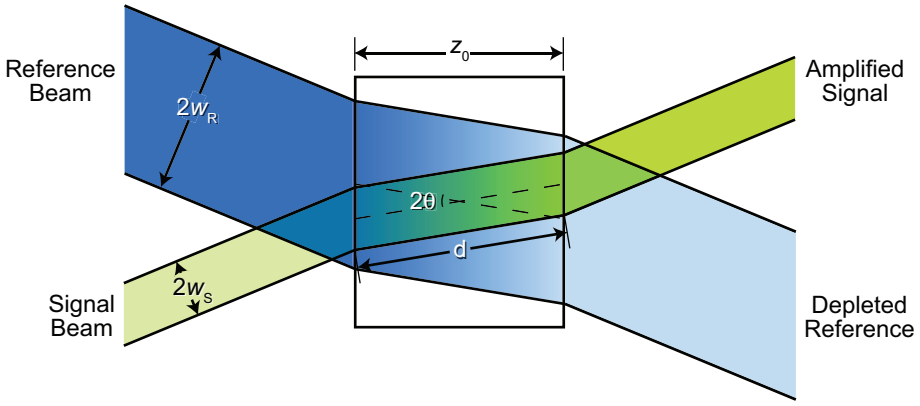

Fig. 4. Photorefractive Amplification Layout.

Using the parameters d for the interaction length within the photorefractive medium ($d = z_0/\cos\theta$ in this layout), 2θ for the angle between the signal and reference beams (inside the photorefractive medium), $\Delta\theta$ for the divergence (or convergence) angle of the signal beam (we assume the reference is a perfect plane wave), and define the grating contrast as

$$m \equiv 2\cos 2\theta \frac{\sqrt{I_R I_S}}{I_R + I_S} \approx 2\cos 2\theta \sqrt{\frac{I_S}{I_R}}, \tag{12}$$

where I_R and I_S are the irradiances of the reference and signal beams respectively, we find the amplification to be

$$g_{pr} = 1 + \frac{1}{m^4} \frac{n_1^2}{n_1^2 + \Delta\theta^2 \tan^2 2\theta} \sin^2\left(\frac{\pi d}{\lambda \cos\theta} \sqrt{n_1^2 \cos^2 2\theta + \Delta\theta^2 \sin^2\theta} \right). \tag{13}$$

Eq. (13) contains three parts: (1) the unity amplification expected under conditions under which there is no energy transfer, a $1/m^4$ factor describing the maximum amplification [an approximation to $\left(1 - \sqrt{1-m^2}\right)^{-2}$], and an efficiency portion involving n_1 and $\Delta\theta$. The angular acceptance can be calculated from this efficiency factor, but there is still

amplification at angles outside the acceptance angle. Fig. 5 shows an example of efficiency using parameters that match our experiment: $\Delta n \approx 5.63\times10^{-4}$, $\theta = 165$ mr (calculated from outside angle of 22.5° and refractive index of 2.33), $d = 4.06$ mm (crystal thickness 4.00 mm), $\lambda = 488.0$ nm. The initial cutoff—what could normally be considered the half acceptance angle—is 1.68 mr. Nonetheless, the efficiency exceeds 5% of maximum at angles as large as 4.25 mr, more than 2.5× greater than the normal definition of acceptance angle.

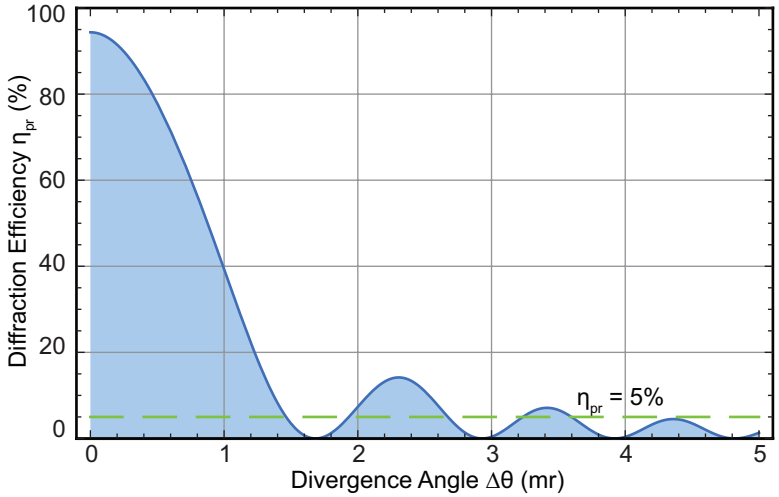

Fig. 5. Photorefractive Acceptance Angle for 4.0-mm Crystal.

Another important fact is that the diffraction efficiency—and its values at higher divergence angles—is dependent on the interaction length. If the crystal thickness is changed from 4.00 mm to 4.50 mm, the resulting diffraction efficiency plot becomes that shown in Fig. 6.

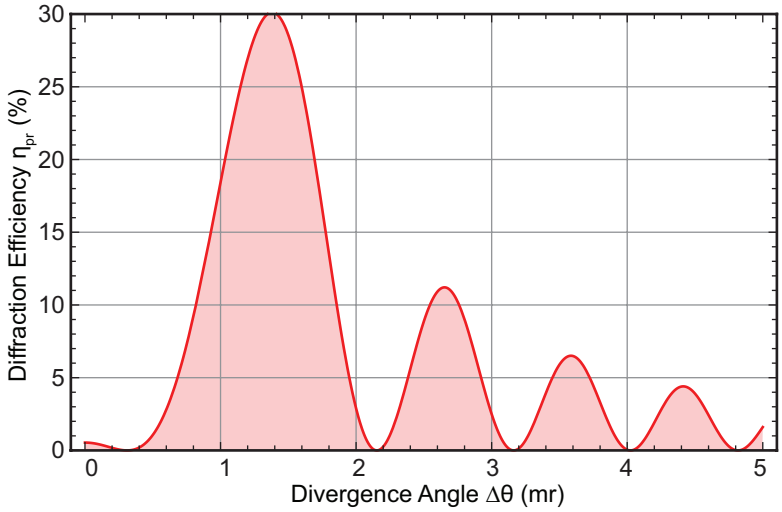

Fig. 6. Photorefractive Acceptance Angle for 4.5-mm Crystal.

Wavelength shifts can have the same effect as divergence. Assuming the signal beam diameter is 2 mm, for the experiment described above, the signal beam divergence angle will be 156 μr. This system will have significant amplification even at wavelengths 25 nm away from the reference beam. Fig. 7 shows the amplification over this bandwidth, which (based on 488 nm illumination) corresponds to a frequency shift of 30 THz. Note that, in our initial experiments mentioned above, we saw amplification of a signal centered 80 nm away from the reference. This model indicates that, with the pump at 532 nm, an input signal at 612 nm would generate an output at 532 nm with approximately 40% the irradiance of the signal.

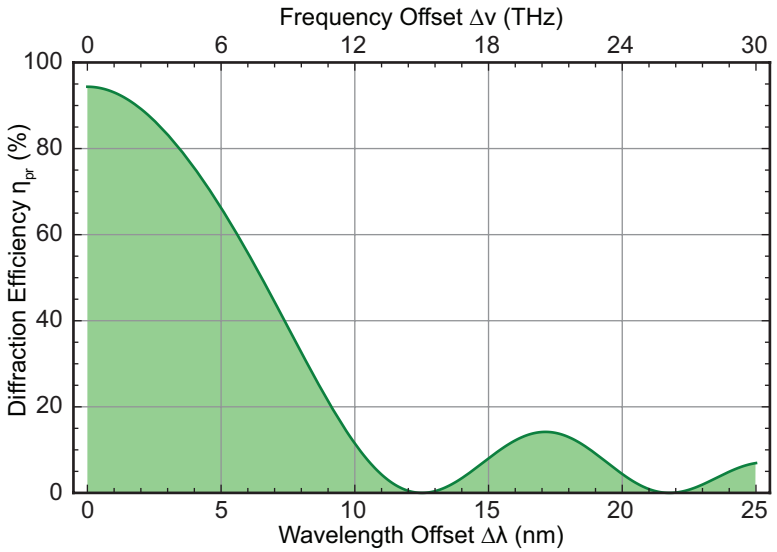

Fig. 7. Photorefractive Amplification Bandwidth.

3. Experiment

As described above, we performed two sets of experiments. The first, which has been referred to as the initial experiments, used a reference beam at 532 nm, and was a three-wave mixing experiment. The second used reference at 488 nm and was a pure two-wave mixing experiment, with the signal having either frequency or phase modulation.

3.1. Three-Wave Experiment

The experiment at 532 nm used the setup shown in Fig. 8. The reference laser was a frequency-doubled Nd:YVO_4 laser operating at 532.1 nm with a beam diameter of 2 mm, operating in single longitudinal mode with a linewidth of 5 kHz. The beamsplitter transmitted 98% of the reference, reflecting 2%. Half of this beam was reflected by the 50% mirror, forming the coherent signal, whose power was 1% of the original beam. In the absence of output from the non-coherent laser, interference between the reference and the coherent signal formed a photorefractive grating in the crystal.

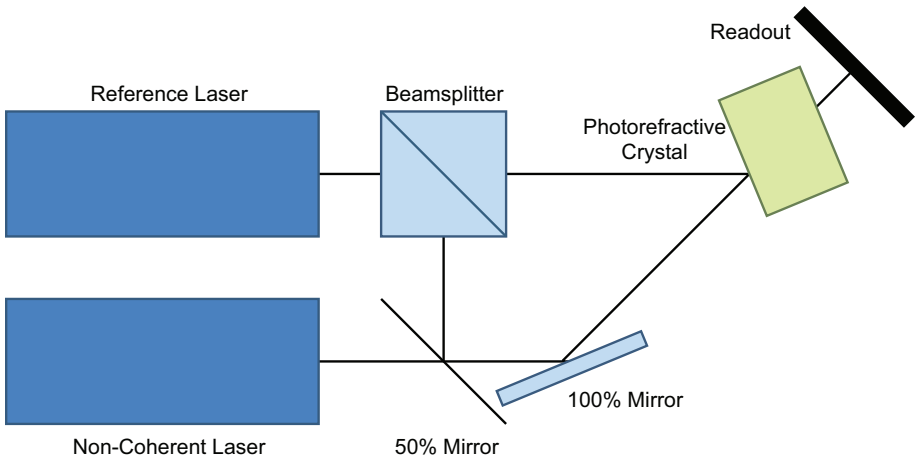

Fig. 8. Layout of Preliminary Experiment.

The non-coherent laser generated one of five other signals: (1) 532 nm from another doubled Nd:YVO_4 laser, not coherent with the reference; (2) 543 nm from a green HeNe laser; (3) 594 nm (yellow) from another HeNe laser; (4) 612 nm from the same HeNe laser as the 594-nm signal; and (5) 633 nm from another HeNe laser. Results of the

amplification experiment appear in Table 1. The model was relatively accurate in predicting amplification at wavelengths close to the reference, but underestimated the amplification at longer wavelengths. In particular, the model predicted amplification at 594 nm to be less than half amplification for a 543-nm signal, but measurements showed the two amplifications to be nearly the same.

Table 1. Amplification in Preliminary Experiment.

Non-Coherent Laser Wavelength	Raw Amplification	532-nm Amplification	Predicted 532-nm Amplification
532 nm	42	41	41.3
543 nm	2.3	1.3	1.34
594 nm	2.4	1.4	0.55
612 nm	1.7	0.7	0.35
633 nm	1.0	0	0.03

The most important output of this experiment, however, is the amplification of an *independent, non-coherent signal* at the same nominal wavelength as the reference. This demonstrates that, with three-wave mixing, where a static photorefractive grating is created, a completely independent signal can be amplified, agreeing with Fig. 7. This experiment demonstrated that a low-SNR signal from a separate source can be amplified, even though it is not coherent with the reference, when three-wave mixing is used. There are significant applications in the communications field.

3.2. Four-Wave Experiment

To demonstrate the capability of the Fast Photorefractive Effect to measure vibration, a four-wave mixing experiment was performed. In this case, the reference was an Ar^+ ion laser operating in single-frequency mode at 514.5 nm, with a linewidth of 1 MHz. The layout of this experiment is shown in Fig. 9. In this experiment, the beam from the laser first passed through a beamsplitter, separating it into reference (90% of the power) and signal (10% of the power) beams. The reference then was directed to a Cu:KNSBN crystal which was used in phase conjugation mode. A mirror on the other side of the crystal retroreflected the portion of the reference that passed through, interference between the forward and retroreflected portions forming a static grating in the crystal along its *c*-axis. The signal reflected from a mirror mounted on a piezoelectric transducer (PZT). That beam passed through a 50-50 beamsplitter before encountering the KNSBN crystal. The reflected half of the signal was then retroreflected to illuminate a detector. The transmitted half struck the KNSBN crystal, and a photorefractively amplified phase conjugate signal was produced, traveling back along the original signal path. Half of this beam was directed to the detector, where it formed an interference pattern with the portion of the signal that was retroreflected. Temporal variations in the interference pattern were captured by the detector and interpreted as signals at nonzero frequency.

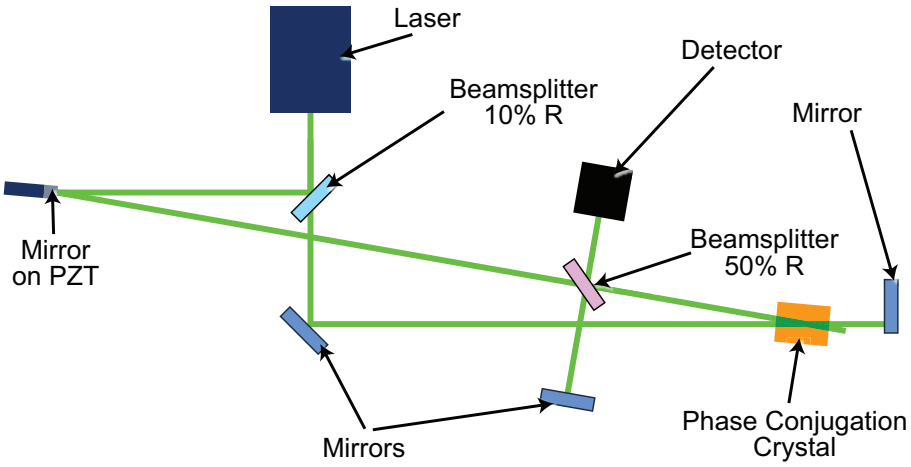

Fig. 9. Optical Layout of Four-Wave Experiment.

Motion of the PZT was adjustable. At the highest frequency we could use, 10 kHz, full-range motion was limited to about ±1 μm, and we restricted the motion at other frequencies to match it. Driving the PZT at 1 Hz for a baseline comparison, we found a phase conjugate signal similar to what we expected, with the highest peak at dc, strong peaks at

2 and 4 Hz, and slightly weaker peaks at 1 and 5 Hz (Fig. 10). The exact predicted response would have had stronger peaks at 1 Hz, with the response decreasing at higher frequencies.

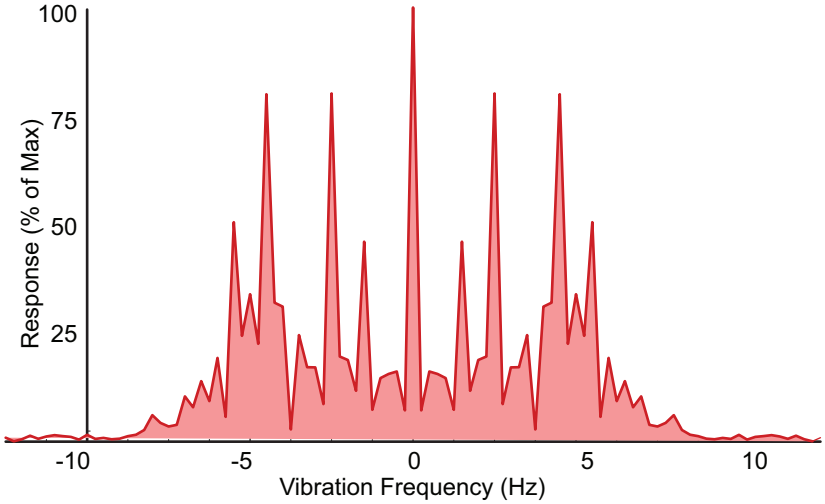

Fig. 10. Frequency Response of Four-Wave Mixing Experiment at 1 Hz.

To test the vibration measurement capabilities, these experiments were repeated at PZT drive frequencies of 10 Hz, 100 Hz, 10 kHz, and 100 kHz (Fig. 11). Again, the results were similar to predictions. At PZT drive frequencies of 10 Hz and 10 kHz, the response is almost exactly what we would predict. At 100 Hz, there are some artifacts at lower frequencies (~25 Hz), surrounding the three large peaks at dc and ±100 Hz. The 1-kHz test shows a pattern similar to that shown in the 1-Hz experiment (Fig. 10), where the even-numbered peaks are stronger than the odd-numbered peaks. At 10 kHz, the peaks fit nearly a perfect Bessel function.

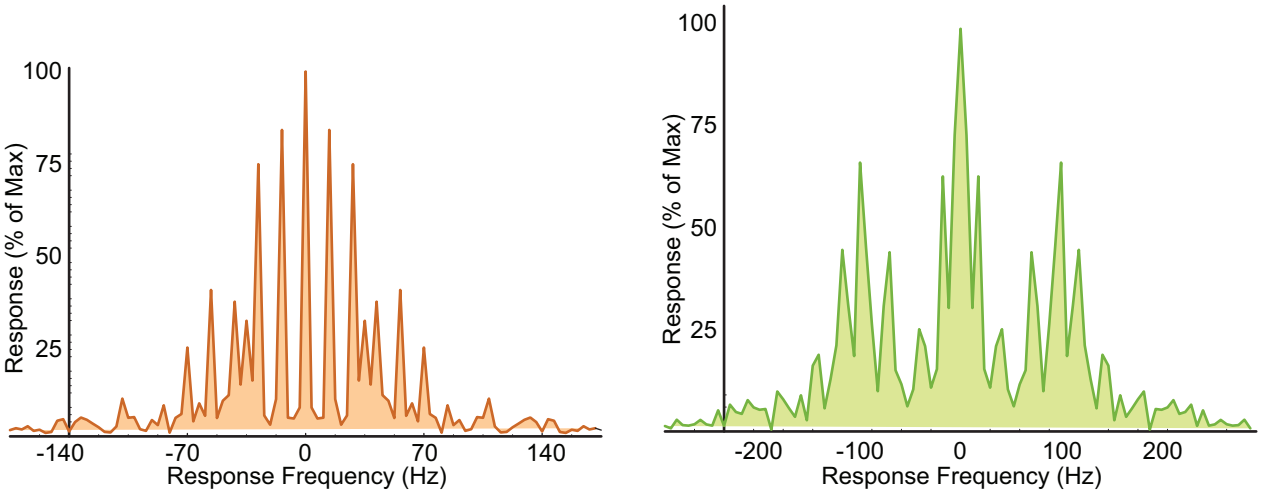

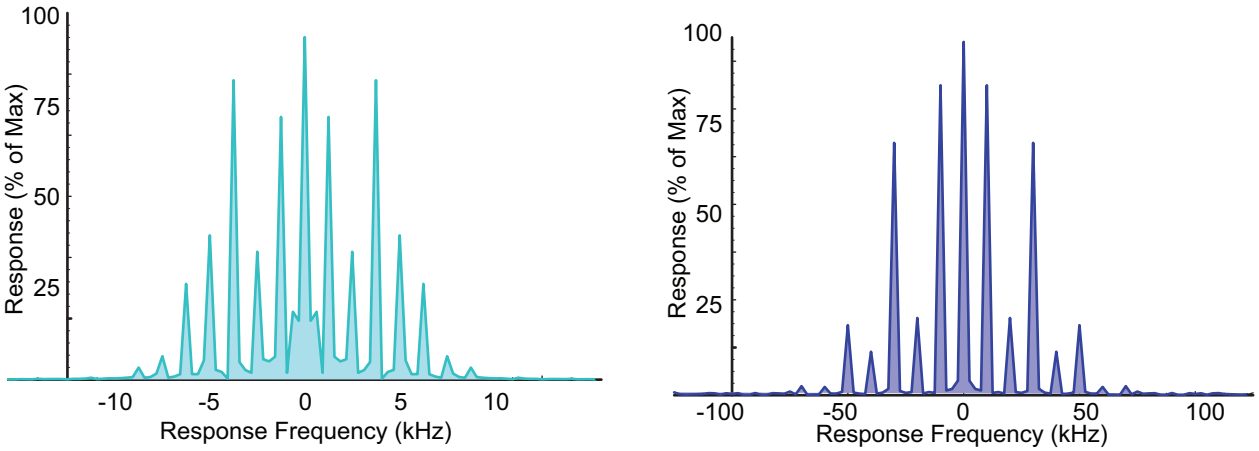

Fig. 11. Four-Wave Amplification of Vibration Signals at (a) 10 Hz, (b) 100 Hz, (c) 1 kHz, and (d) 10 kHz.

We attribute the addition peaks at 100 Hz to vibration; the same results were seen using just the raw signal and the mirror. The different shapes of the responses, where some harmonics are deemphasized, is the result of specific amplitudes and phases of the vibrational signal. Eq. (11) lists the m^{th} Fourier coefficient of the vibrational signal as $J_m(ka)$, where k is the propagation constant and a is the vibrational amplitude. Different orders of the Bessel function have zeroes at different locations, so the coefficients could be reduced. In addition, the analysis was specifically for vibration as a sine function. The constant phase could change this to a cosine or a combination of the two, which would affect which coefficients are large and which are small. In any case, this experiment demonstrated clear capture of vibrational signatures up to 10 kHz using photorefractivity in a four-wave configuration. The 10-kHz limit was imposed by the PZT, not the optical system.

3.3. Two-Wave Experiment

Another experiment was performed, this time with the reference laser operating at 488.0 nm (Ar^+ ion laser). Its beam diameter was 2 mm and its linewidth was 3 GHz. We tested a photorefractive crystal, Cu:KNSBN, under illumination at 488.0 nm from a single-frequency argon laser. The crystal chemistry was studied by electron diffraction spectroscopy at the University of California, Irvine, spectroscopy facility, and determined to have the formula $(K_{0.45}Na_{0.55})_{0.16}(Sr_{0.78}Ba_{0.22})_{0.92}Nb_2O_6$. In other words, using the standard formula listed in Section 1, the parameters are $x = 0.45$, $a = 0.08$, and $y = 0.78$. We measured the refractive indices at 488.0 nm to be $n_e = 2.33234 \pm 0.00558$ and $n_o = 2.38091 \pm 0.01851$. The linear electro-optic coefficients are $r_{13} = 50$ pm/V, $r_{42} = 400$ pm/V, and $r_{33} = 270$ pm/V[16]. We measured the mass density of the crystal to be 6.33 g/cm^3. The Cu doping was nominally 0.04% by weight, corresponding to Cu^+ ion density of 1.92×10^{19} cm^{-3}. The crystal measured 4 mm × 5 mm × 6 mm, with its c-axis along the 6-mm length. All experiments were performed at controlled room temperature, 297K.

The experimental layout is shown in Fig. 12. Each beam made an angle of $\pi/8$ (22.5°) with the normal to the crystal face. Based on this and the measure refractive index, the angle each beam made with the surface normal inside the crystal was 165 mr (9.45°). The beams were polarized in the plane of incidence, resulting in a photorefractive grating whose gradient was in the same direction as the crystal optical axis, and ensuring that the refractive index to be used was the extraordinary index. The irradiance of the reference beam, I_0, was 8.15 W/cm^2 and that of the signal beam, I_1, was 97.8 mW/cm^2. The expected interference pattern contrast, then, was 0.216.

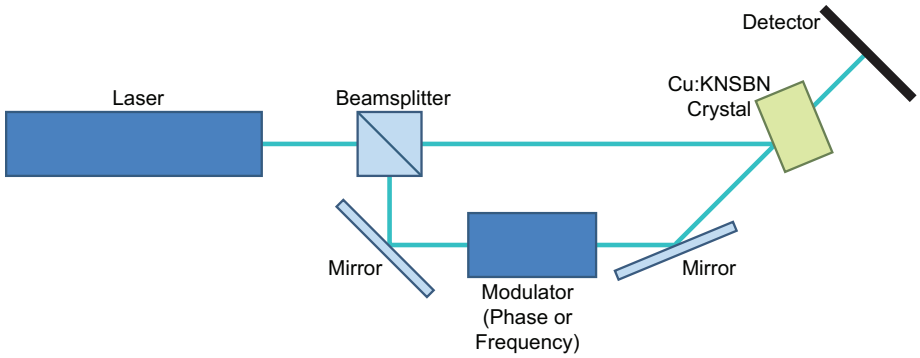

Fig. 12. Layout of Modulation Experiment.

Given the material and layout parameters, single-pass amplification of ~35 was predicted for the beam without frequency shifting. Our measurements showed steady-state amplification of 33.5, well within the experimental error. When we blocked the reference beam, then observed the amplified signal as we unblocked the reference, we determined that the amplification had a response time of 0.2323 s (from 0 to 1-e^{-1} of final output). From this we estimated that, with total input irradiance $I_0 + I_1 = 8.25$ W/cm^2, amplification of signals with frequencies slightly different from that of the reference would have a bandwidth of 4.305 Hz.

We then tested the response using a pure frequency shift. We ran a logarithmic sweep from $\Delta\nu = 0$ to 20 Hz. Traditional photorefractive modeling predicted that amplification would drop exponentially with frequency shift. The gain of this system matched the exponential model to an accuracy of 98.6% (Fig. 13), and the exponential decay corresponded to the predicted 4.3-Hz bandwidth.

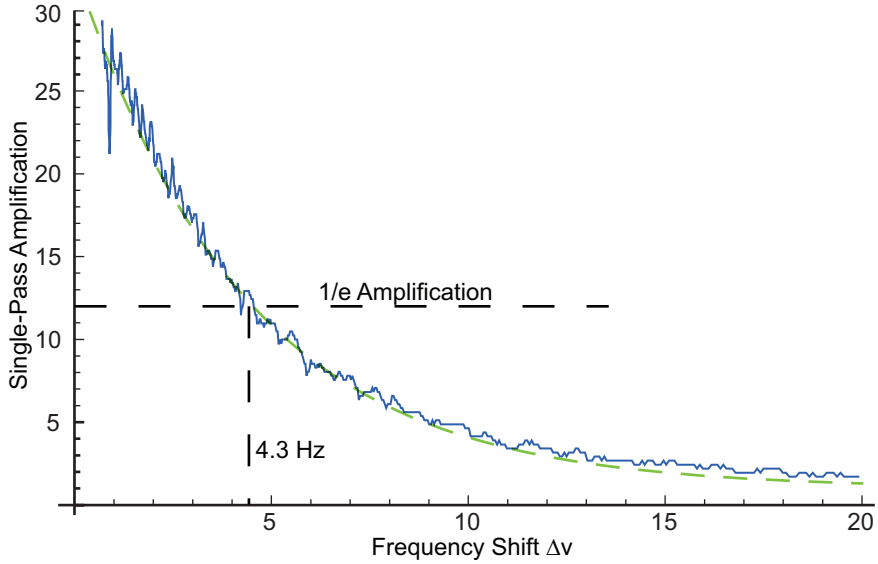

Fig. 13. Measured (Solid Line) and Modeled (Dashed Line) Photorefractive Frequency Response.

We then repeated the experiment, but instead of modulating the frequency we used a phase modulator. Thus, instead of a frequency shift, we generated a pure phase shift, modulating the phase with a sine wave. We anticipated that the phase modulation signal would be relatively constant. We therefore kept the maximum phase modulation constant at ~3 radians (purposely modulating it less than 180°). The phase modulation frequency was also scanned from 0 to 20 Hz (Fig. 14), and the modulation signal showed no significant deviation from the constant value. The effective amplification of this part of the signal was ~33.

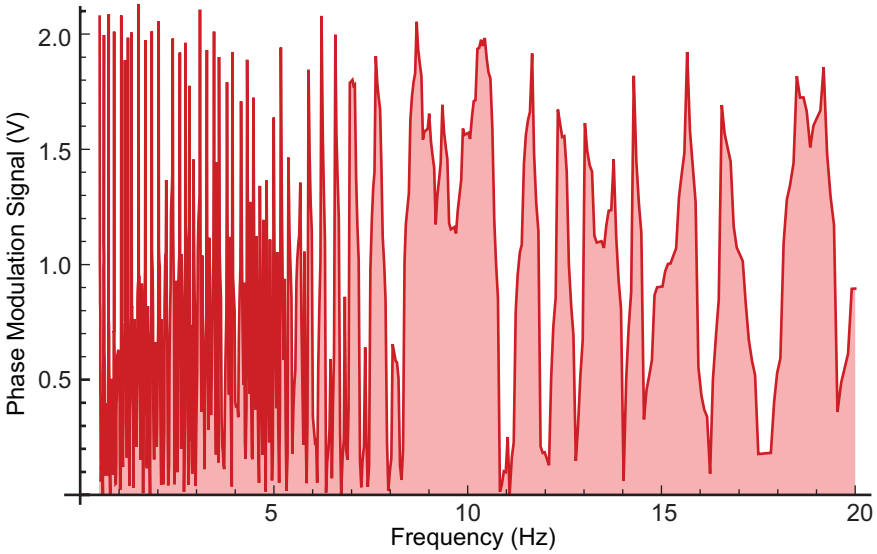

Fig. 14. Amplification of a Phase Modulated Signal.

The parameters of this experiment, assuming diffusion limit, indicate that the internal electric field amplitude is E_{sc} = 3.57 V/cm, resulting in a refractive index modulation of 5.215×10^{-4}. The Kogelnik model predicts an acceptance angle of 0.529 mr (1.79 arc minutes), wavelength acceptance of 0.661 nm, and amplification bandwidth of 832 GHz. This was far beyond our measurement capabilities. We were able to drive our phase modulator up to 4 MHz without significant loss of modulation depth (Fig. 15). Over this range, the gain was 32 within ±3%, plus one dip around 1.1 MHz. Even that dip was only to 29.5, 8% below the average gain.

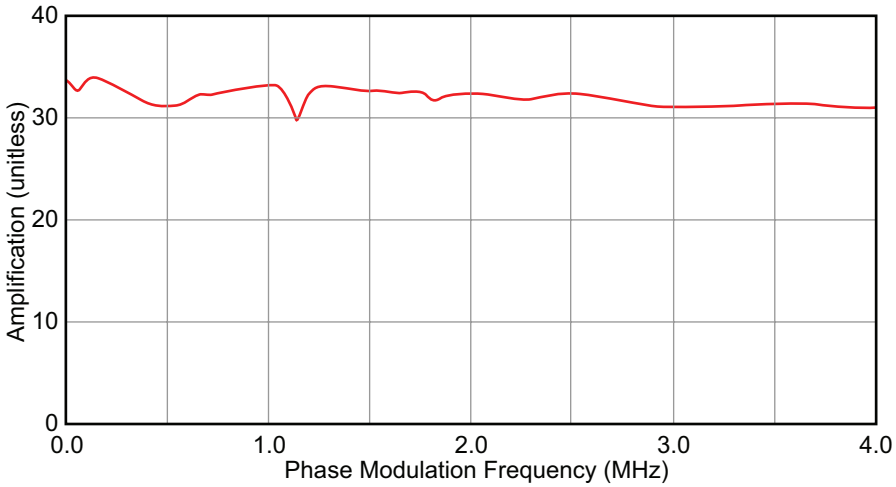

Fig. 15. Photorefractive Amplification at High Frequency.

This experiment demonstrated that the phase modulation model using Jacobi-Anger expansion is correct, since phase-modulated signals at up to 4 MHz were amplified within 5% of the dc gain, while frequency-modulated signal amplification decayed with frequency with the expected exponential signature. The bandwidth matched the prediction to within experimental error. The experiment also demonstrated that even high-frequency phase-modulated signals can be amplified with a photorefractive system. This has direct application to vibrometry.

4. Summary and Conclusions

We have demonstrated high-quality photorefractive amplification at frequencies that would normally be considered much too high for use in photorefractivity. In three experiments—one using two-wave mixing, another with three-

wave, and the third with four-wave mixing—we were able to demonstrate photorefractive amplification of a pure vibrational signature at up to 10 kHz, a phase modulation signal (modeling a vibrational signature) at up to 4 MHz, and of non-coherent, external signals at frequency offsets up to 73 THz. We present a model of how this works, whether in two-wave mixing (phase-modulated and vibration signals only), or three-wave or four-wave mixing (vibration, phase-modulated, and frequency-modulated signals). The model fit is relatively good. These experiments have shown that the Fast Photorefractive Effect is useful for photorefractive amplification at high frequencies, and could be useful in a multitude of field, such as vibration testing and communications.

5. References

1. P. Yeh, "Theory of Unidirectional Photorefractive Ring Oscillators," *J. Opt. Soc. Am. B* **2**(12)**,** 1924-1928 (1985).
2. S. Breugnot, H. Rajbenbach, M. Defour, and J.P. Huignard, "Low-Noise Photorefractive Amplification and Detection of Very Weak Signal Beams," *Opt. Lett.* **20**(5)**,** 447-449 (1995).
3. I. Lahiri, L.J. Pyrak-Nolte, D.D. Nolte, M.R. Melloch, R.A. Kruger, G.D. Bacher, and M.B. Klein, "Laser-Based Ultrasound Detection Using Photorefractive Quantum Wells," *Appl. Phys. Lett.* **73**(8)**,** 1041-1043 (1998).
4. F. Vachss, C. Gu, J.H. Hong, and T.Y. Chang, "Fundamental Noise Limits in Photorefractive Systems," in *Photorefractive Materials, Effects, and Devices*, *Proc. OSA* **14**, pp. 92-96 (1991).
5. P. Yeh, "Fundamental Limit of the Speed of Photorefractive Effect and Its Impact on Device Applications and Material Research," *Appl. Opt.* **26**(4)**,** 602-604 (1987).
6. S. Ducharme and J. Feinberg, "Speed of the Photorefractive Effect in a $BaTiO_3$ Single Crystal," *J. Appl. Phys.* **56**(3)**,** 839-842 (1984).
7. R.M. Kurtz, W. Lu, J. Piranian, T. Jannson, and A.O. Okorogu, "The Fast Photorefractive Effect and Its Application to Vibrometry," *J. Holography Speckle* **5**(2)**,** 149-155 (2009).
8. H. Zhang, B. Guo, H. Jiang, Y. Shih, and L. Yan, "Characterization of the KNSBN:Cu Crystal with Two-Wave Coupling at Visible and Infrared Wavelengths," *App. Phys. B* **61**(207-211 (1995).
9. R.M. Kurtz, A.O. Okorogu, J. Piranian, T.C. Forrester, and T.P. Jannson, "High-Frequency Photorefractive Amplification for ATR Applications," in *Photorefractive Fiber and Crystal Devices: Materials, Optical Properties, and Applications XI*, *Proc. SPIE* **6314**, p. 63140O (2006).
10. B.F. Pouet, R.K. Ing, S. Krishnaswamy, and D. Royer, "Heterodyne Interferometer with Two-Wave Mixing in Photorefractive Crystals for Ultrasound Detection on Rough Surfaces," *Appl. Phys. Lett.* **69**(25)**,** 3782-3785 (1996).
11. N.V. Kukhtarev, V.B. Markov, S.G. Odulov, M.S. Soskin, and V.L. Vinetskii, "Holographic Storage in Electrooptic Crystals. I. Steady State," *Ferroelectrics* **22**(949-960 (1979).
12. N.V. Kukhtarev, V.B. Markov, S.G. Odulov, M.S. Soskin, and V.L. Vinetskii, "Holographic Storage in Electrooptic Crystals. II. Beam Coupling—Light Amplification," *Ferroelectrics* **22**(961-964 (1979).
13. N.V. Kukhtarev, T. Kukhtareva, S.F. Lyuksyutov, M.A. Reagan, P.P. Banerjee, and P. Buchhave, "Running Gratings in Photoconductive Materials," *J. Opt. Soc. Am. B* **22**(9)**,** 1917-1922 (2005).
14. F.W.J. Olver, D.W. Lozier, R.F. Boisvert, and C.W. Clark, eds., *NIST Handbook of Mathematical Functions*, Cambridge University Press, New York, NY (2010).
15. H. Kogelnik, "Coupled Wave Theory for Thick Hologram Gratings," *Bell Sys. Tech. J.* **48**(9)**,** 2909-2947 (1969).
16. J. Quanzhong, L. Xinliang, S. Yongyuan, S. Daliang, and C. Huanchu, "Copper-Ion Point Defects in the Photorefractive Material $(K_xNa_{1-x})_{0.4}(Sr_yBa_{1-y})_{0.8}Nb_2O_6$," *Phys. Rev. B* **50**(6)**,** 4185-4188 (1994).